

Geophysical Research Letters[®]



RESEARCH LETTER

10.1029/2022GL102058

Key Points:

- Dynamically modeled atmosphere-to-ocean soluble iron deposition permits deposition driver variability to affect upper ocean biogeochemistry
- Tropical Pacific iron deposition increases with radiative forcing, affecting phytoplankton nutrient limitation, production, and POC flux
- Deposition increases align with soil moisture decreases in adjacent land areas, and precipitation increases over the equatorial Pacific

Supporting Information:

Supporting Information may be found in the online version of this article.

Correspondence to:


E. J. Drenkard,
liz.drenkard@noaa.gov

Citation:

Drenkard, E. J., John, J. G., Stock, C. A., Lim, H.-G., Dunne, J. P., Ginoux, P., & Luo, J. Y. (2023). The importance of dynamic iron deposition in projecting climate change impacts on Pacific Ocean biogeochemistry. *Geophysical Research Letters*, 50, e2022GL102058. <https://doi.org/10.1029/2022GL102058>

Received 2 DEC 2022
Accepted 7 SEP 2023

The Importance of Dynamic Iron Deposition in Projecting Climate Change Impacts on Pacific Ocean Biogeochemistry

Elizabeth J. Drenkard¹ , Jasmin G. John^{1,2} , Charles A. Stock¹ , Hyung-Gyu Lim^{3,4,5} , John P. Dunne¹ , Paul Ginoux¹ , and Jessica Y. Luo¹ 

¹NOAA/OAR/GFDL, Princeton, NJ, USA, ²NOAA/OAR/AOML, Key Biscayne, FL, USA, ³Atmospheric and Oceanic Sciences Program, Princeton University, Princeton, NJ, USA, ⁴Scripps Institution of Oceanography, University of California San Diego, La Jolla, CA, USA, ⁵Korea Institute of Ocean Science and Technology, Busan, South Korea

Abstract Deposition of mineral dust plays an important role in upper-ocean biogeochemical processes, particularly by delivering iron to iron-limited regions. Here we examine the impact of dynamically changing iron deposition on tropical Pacific Ocean biogeochemistry in fully coupled earth system model projections under several emissions scenarios. Projected end-of-21st-century increases in central tropical Pacific dust and iron deposition strengthen with increasing emissions/radiative forcing, and are aligned with projected soil moisture decreases in adjacent land areas and precipitation increases over the equatorial Pacific. Increased delivery of soluble iron results in a reduction in, and eastward contraction of, equatorial Pacific phytoplankton iron limitation and shifts primary production and particulate organic carbon flux projections relative to a high emissions projection (SSP5-8.5) wherein soluble iron deposition is prescribed as a static climatology. These results highlight modeling advances in representing coupled land-air-sea interactions to project basin-scale patterns of ocean biogeochemical change.

Plain Language Summary We use an Earth System Model (ESM) to explore climate-driven changes in the deposition of dust and iron from the atmosphere to the ocean under a range of climate change scenarios. These simulations use a “dynamic” approach for iron deposition which means iron deposition is affected by changing atmospheric dust loads and factoring in wind and precipitation which affect dust and iron transfer from the atmosphere to the ocean. Under increasing climate change scenarios, GFDL’s ESM4.1 projects drier soil conditions, as well as more dust in the atmosphere and precipitation over the Pacific Ocean toward the end of the 21st century. Elevated levels of future iron delivery to the ocean reduce iron limitation of phytoplankton growth in the central Pacific. As a result, we find higher levels of phytoplankton production in the central, equatorial Pacific but lower levels downstream in the western and off-equatorial Pacific because other nutrients necessary for growth are depleted by reduced upwelling and enhanced production in the eastern Pacific. This geographic pattern also appears in the change in carbon sinking from the surface ocean to depth. Overall, these results highlight how ESM advances can improve our understanding of climate change impacts on marine ecosystems.

1. Introduction

Iron availability in the surface ocean affects primary productivity, particularly in regions where iron scarcity limits phytoplankton growth (i.e., High-Nitrate-Low-Chlorophyll (HNLC) areas; C. M. Moore et al., 2013). This availability is governed by a number of input, transport and transformation processes (Hamilton et al., 2020b; Tagliabue et al., 2017). Iron is sourced from the seafloor as hydrothermal (Tagliabue et al., 2010) and sediment fluxes (Elrod et al., 2004), from land as runoff (Krachler et al., 2005), and atmospheric deposition of terrestrial (Mahowald et al., 2005) and extraterrestrial (Johnson, 2001) dust. Ocean iron concentrations are further affected by atmosphere (i.e., deposition location; Duce & Tindale, 1991) and ocean (e.g., upwelling and advection; Lim et al., 2022) circulation, and scavenging and remineralization (e.g., Tagliabue et al., 2014).

This study focuses on the impact of climate-driven changes in deposition of terrestrial dust, which is an important source of iron to the low-latitude, open ocean (Tagliabue et al., 2017). Atmospheric deposition occurs through gravitational or turbulence-driven settlement, and/or precipitation of atmospherically suspended and transported particulates (Duce & Tindale, 1991; Evans et al., 2016; Schulz et al., 2012). A limited amount of the iron from these particulates is dissolved and subsequently available for biological utilization by phytoplankton for essential

© 2023 The Authors. This article has been contributed to by U.S. Government employees and their work is in the public domain in the USA.

This is an open access article under the terms of the [Creative Commons Attribution License](https://creativecommons.org/licenses/by/4.0/), which permits use, distribution and reproduction in any medium, provided the original work is properly cited.

metabolic processes (Baker & Croot, 2010). The ability for iron to stimulate phytoplankton productivity in HNLC regions has been demonstrated through iron fertilization experiments (e.g., Boyd et al., 2000; Coale et al., 1996) and has been hypothesized as an important mechanism for removing CO₂ from the atmosphere on glacial-to-interglacial time scales (Martin, 1990).

The amount of dust emitted from a terrestrial region broadly depends on aeolian erodibility (e.g., soil texture, dryness, and bareness) of the substrate and its wind exposure (Gillette & Passi, 1988). These surface characteristics are susceptible to changing climate conditions such as rising surface air temperature and precipitation shifts, as well as anthropogenic land-use practices (Burrell et al., 2020). In projecting environmental risks of climate change, the scientific community employs shared socioeconomic pathways (SSPs, O'Neill et al., 2014), which outline different scenarios given possible global policies and economic development over the next century. Of these, the highest greenhouse gas emissions and radiative forcing scenario (SSP5-8.5) presents the greatest potential for climate non-stationarity, including the largest increase in global mean temperatures (Lee et al., 2021) and global risk of desertification (Huang et al., 2020), attributable in part to redistribution of global precipitation (Lee et al., 2021), and land-use changes, such as reduction in forest and pasture area (Riahi et al., 2017).

Earth System Models (ESMs) facilitate study of the climate system and its impact on, and interactions with, ocean biogeochemical (BGC) processes. Unique to several ESM contributions to the Sixth Coupled Model Inter-comparison Project (CMIP6) is the dynamic coupling of atmospheric dust emissions and deposition with climate conditions (Danabasoglu et al., 2020; Dunne et al., 2020; Hajima et al., 2020; Sellar et al., 2019). Specifically, the simulated amount of mineral aerosol transferred from the atmosphere to the ocean reflects both the amount of dust emitted into the atmosphere model from the land, and processes such as precipitation that remove dust from the atmosphere (Evans et al., 2016). This is in contrast to earlier CMIP ESM contributions that parameterized iron deposition as a preindustrial or historical climatology, an approximation that omits the role of interannual and multidecadal dust variability in ocean BGC processes (Lim et al., 2022; Séférian et al., 2020).

Here we use a fully coupled global ESM (NOAA GFDL's ESM4.1, Dunne et al., 2020) run for a range of greenhouse gas emissions scenarios to investigate the role of dynamic dust and soluble iron deposition (referred to hereafter as "dynamic deposition") in driving future conditions in global ocean nutrient limitations by comparing dynamic results against simulations where iron deposition is maintained as a static climatology. In contrast with previous studies which considered offline estimates of changing iron supply (e.g., Hamilton et al., 2020a; J. K. Moore et al., 2004), GFDL ESM4.1 provides an opportunity to assess interactions between self-consistent and simultaneous changes in dust supply, atmospheric transport, meteorology and ocean processes across climate change scenarios. We note, however, that unlike Hamilton et al. (2020a), our analysis is restricted to changes in natural dust sources, omitting direct contributions from fire and industrial sources.

2. Methods

2.1. ESM4.1 Model and Simulations

Calculations of dust emissions in ESM4.1 incorporate friction velocity, soil moisture, surface bareness, and land use (Evans et al., 2016). Dust sources can either increase or decrease depending on both climate and land use changes. Source expansion by land use can be related to deforestation, grazing, or cultivation, and by drought or wildfires due to climate change. Source reduction may be due to land use practices such as irrigation, reforestation or land abandonment or vegetation growth by increased precipitation with climate change. All these processes are included in ESM4.1 either dynamically or from land use scenarios.

Suspended mineral aerosols are transported for several days by wind advection and convection before being deposited at the surface by dry and wet removal processes. Dry removal includes both gravitational settling and surface scavenging, while wet removal includes rainout (in-cloud scavenging) and washout (below-cloud scavenging). As described in Stock et al. (2020), deposited dust is assumed to have 3.5% iron, with solubility increasing at lower dust concentrations (Text S1 in Supporting Information S1) in accordance with Baker and Croot (2010). We note that this excludes potential impacts of changing atmospheric acidity on solubility (e.g., Meskhidze et al., 2005). In Figure S1 in Supporting Information S1, the comparison of simulated soluble iron deposition with observations (from Mahowald et al., 2009) indicates that the simulated values are overestimated in remote regions (e.g. along Antarctica) and underestimated near source regions (e.g. Mediterranean sea). The comparison of dust deposition from the same model by Stock et al. (2020) indicates similar biases. Additionally, dust aging, increasing soluble iron with time, may also contribute to these biases.

For the dynamic iron deposition (DD) simulations, we used ESM4.1 output generated for the 6th Coupled Model Intercomparison Project (CMIP6, Eyring et al., 2016; John et al., 2018; Krasting et al., 2018a, 2018b). We assessed projected changes across 4 climate change scenarios following ScenarioMIP (SSP1-2.6, SSP2-4.5, SSP3-7.0, and SSP5-8.5, O'Neill et al., 2016). For the high emissions scenario (SSP5-8.5), we also generated a static deposition (SD) control simulation where ESM4.1 was run under preindustrial control, historical, and future periods following CMIP6 experimental protocols (Text S2 in Supporting Information S1), however, soluble iron and lithogenic particle deposition to the ocean were prescribed as 300-year (years 51–350), monthly climatologies calculated from the dynamic dust preindustrial control simulation (ESM4.1 piControl, Dunne et al., 2020; Krasting et al., 2018b). In other words, the ocean in all periods of the SD simulations (i.e., preindustrial, historical, future) receives the same fixed pre-industrial monthly climatological deposition of soluble iron and lithogenic material, while the DD simulation receives time evolving deposition fluxes that are fully informed by ESM4.1's evolving dust emissions and dynamics. The forcing of the DD (SSP5-8.5) and SD runs are equivalent in all other respects, thus isolating the impact of dynamic dust changes on ocean biogeochemistry from those associated with other climate change factors.

2.2. Analyses

We assess long-term projected changes in soluble iron deposition, associated drivers of regional deposition patterns, and upper-ocean biogeochemistry across a range of emission scenario projections. Relative changes are calculated as the difference between 40-year averages of future (2061–2100) and historical (1975–2014) conditions divided by the historical mean. A correction for linear drift based on the corresponding time periods of the pre-industrial control simulation was applied to all climatologies (Text S3 in Supporting Information S1).

We also evaluate the distribution of phytoplankton nutrient limitation, to determine whether the availability of macronutrients (nitrogen or phosphorus) or iron limits phytoplankton growth. ESM4.1 nutrient limitation diagnostics are calculated as biomass-weighted averages over the upper 100 m (Orr et al., 2017) using Liebig's Law of the Minimum (Liebig, 1840), as described in Stock et al. (2020). Regions are designated as “weakly iron limited” where iron limitation factors are less than 0.25 below macronutrient limitation.

Subsequent changes in primary production and particle export were assessed with 100 m integrated net primary production (NPP) and particle export (POC) flux at 100 m, respectively. We also considered the effect of dust deposition on dissolved oxygen levels.

3. Results

Under increasing radiative forcing scenarios, DD ESM4.1 simulations project a progressive enhancement of column-integrated dust, dust deposition and iron deposition in the eastern and central equatorial Pacific, with less pronounced relative changes in other regions (Figure 1, rows 3–5). We note that modest absolute change may correspond with large relative changes when they occur in regions with low historical baseline deposition (Figure 1 vs. Figure S2 in Supporting Information S1). Our focus on relative changes in Figure 1 recognizes that iron limitation generally occurs in low iron deposition regions.

Increasing deposition is aligned with intensified soil drying in adjacent and remote land areas and increasing precipitation over the equatorial Pacific (Figure 1, rows 1–2). Accordingly, decomposition of dust and iron deposition into wet and dry components reveal increases in both of these modes of delivery and importance of both precipitation and dust availability in driving changes in deposition (Figure S3 in Supporting Information S1). Enhanced iron delivery drives a shift in phytoplankton nutrient limitation and NPP, with an eastward recession of tropical Pacific iron limitation and larger declines in western tropical and off-equatorial Pacific primary production (Figure 1, rows 6–7).

Comparison of the DD and SD simulations under the high-emission scenario confirms that inclusion of dynamic iron deposition significantly alters projected biogeochemical changes within the equatorial Pacific and extending into adjacent waters (Figures 2 and 3). In the tropical Pacific, iron is the primary nutrient limiting phytoplankton growth for both SD and DD historical conditions (Figures 2a and 2b). Both simulations exhibit latitudinal and eastward contraction of iron-limited regions under SSP5-8.5 (Figures 2c and 2d), but this change is far more pronounced in the DD simulation, where macronutrient limitation dominates in the western Pacific and poleward

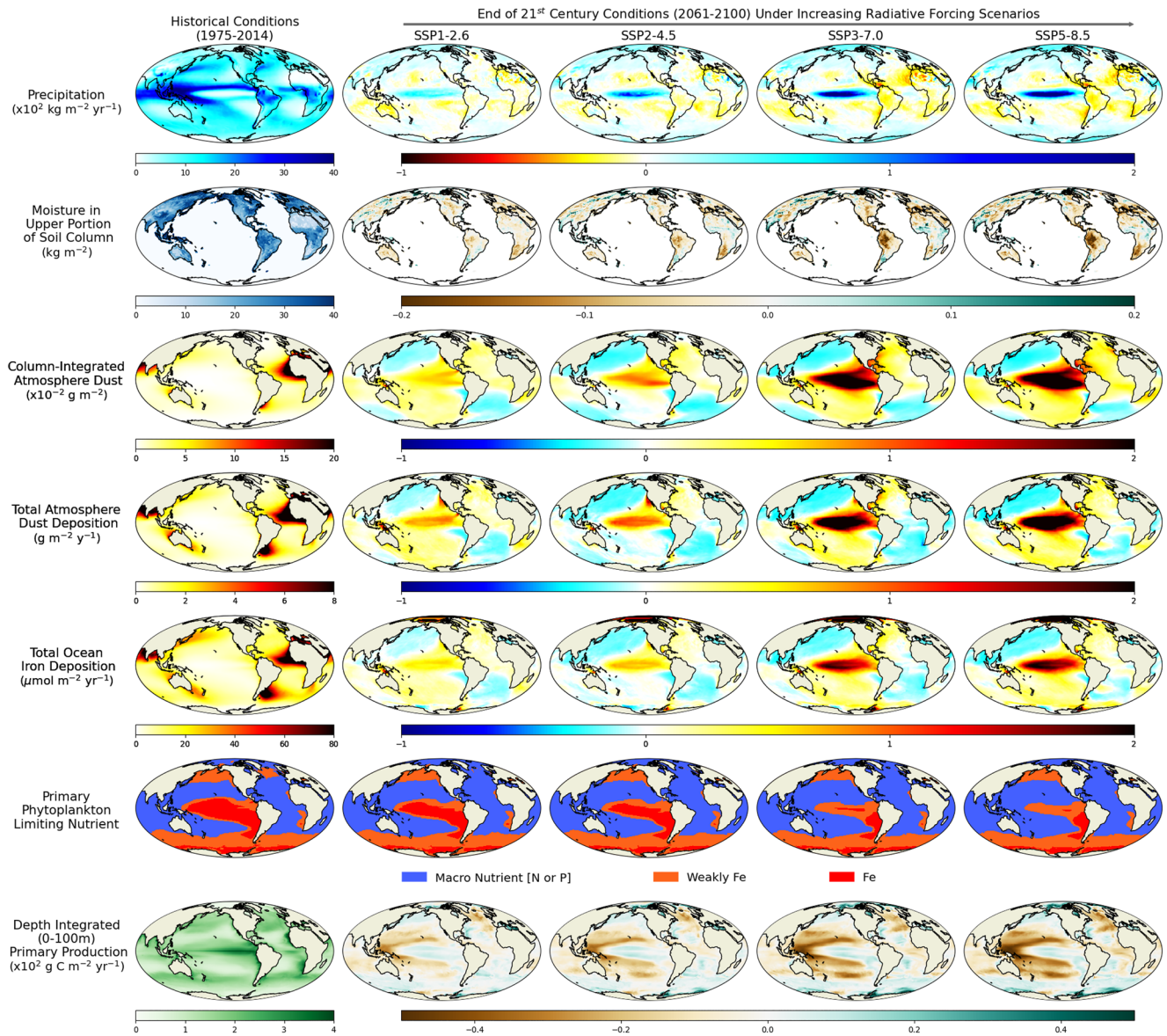


Figure 1. Historical climatologies (left) and relative change (right four columns) in ESM4.1 DD scenario simulations. With the exception of primary phytoplankton limiting nutrient (row 7), all end-of-21st-century-plots show the relative change calculated as (future—historical)/historical, where a value of 0, 1, and 2 indicates no change, a doubling, and tripling of historical conditions, respectively. Conversely, $-1/2$ indicates a halving of historical conditions and -1 indicates where future conditions have gone to 0; values lower than -1 are not physically possible for these diagnostics. The future plots for primary phytoplankton limiting nutrient show the climatological (2061–2100) mean distribution of nutrient limitations.

of 8° latitude by the end of the 21st century. These changes in the distribution of nutrient limitation for both transient simulations exceeds any change attributable to drift or internal variability in the pre-industrial control simulations (Figure S4 in Supporting Information S1).

The distribution of future nutrient limitation in other ocean regions is geographically similar between SD and DD simulations (Figures 2c and 2d). For example, iron limitation appears to be reduced relative to macronutrients in the northern Atlantic Ocean. The appearance of this change in both simulations, however, suggests that it is not attributable to iron deposition mechanism, but rather changing climate conditions (e.g., increased ocean stratification) driving substantial reductions in macronutrient availability (Kwiatkowski et al., 2020), though the projected increase in North Atlantic iron deposition (Figure 1, row 5) would reinforce this shift. Changes in the limiting nutrient can occur due to the most limiting nutrient becoming more abundant, less limiting nutrients becoming less abundant, or a combination of these two mechanisms. The transects in Figure 2 illustrate the

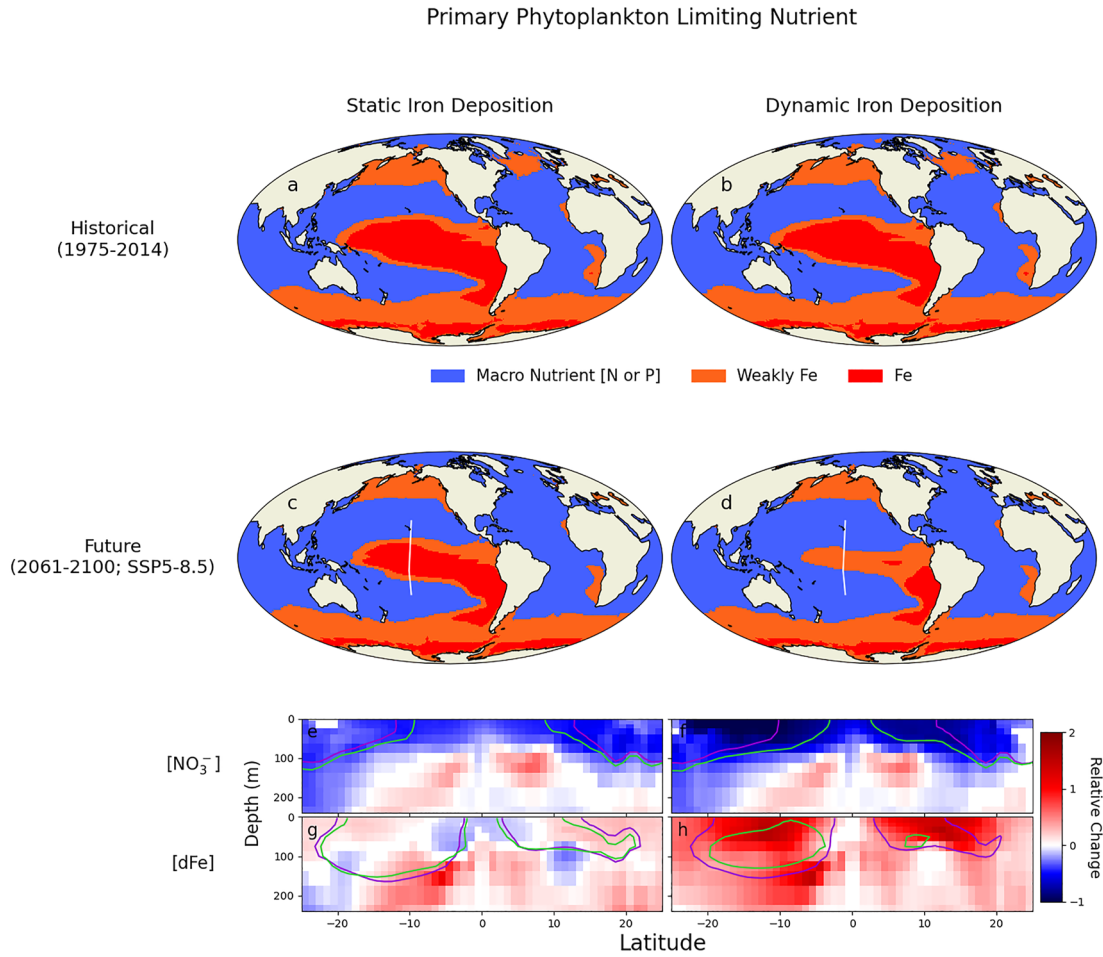


Figure 2. Spatial distribution of the primary phytoplankton limiting nutrients in the ESM4.1 DD and SD simulations (a–d); calculation considers phosphorus (P), nitrogen (N), and iron (Fe). “Weakly Fe” indicates regions where iron limitation approaches (i.e., less than 0.25 below) macronutrient limitation factors (Stock et al., 2020). White lines (c, d) indicate location of transects that show relative change in subsurface concentrations of nitrate ($[\text{NO}_3^-]$; e, f) and dissolved iron (dFe; g, h) for static and dynamic dust simulations. Transect values are masked where future and historical means do not differ significantly (evaluated using a relative student t -test, $p > 0.001$). Purple and green contours indicate the historical and projected future depths, respectively, for $1 \text{ mmol m}^{-3} [\text{NO}_3^-]$ (e, f) and $0.02 \text{ } \mu\text{mol m}^{-3} \text{ dFe}$ (g, h).

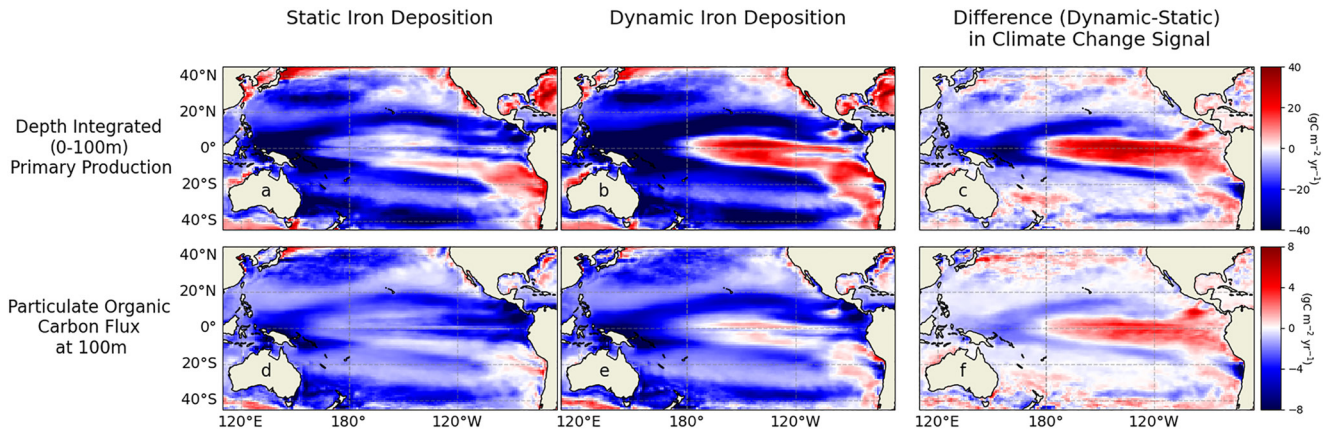


Figure 3. Multi-decadal mean changes (future—historical; color) in integrated upper-ocean (i.e., surface to 100 m) primary production (a, b) and particulate organic carbon flux at 100 m (d, e). The historical mean state is depicted in Figure S5 in Supporting Information S1. Panels (c, f) show the difference between the dynamic and static iron deposition climate change signals for these variables. Panel labels appear on the Australian continent.

relative changes in concentration of nitrate (e, f) and dissolved iron (g, h). Decline in nitrate concentrations above 100 m (e, f) occurs over most of the transect in both SD and DD but is more pronounced (i.e., darker blue) in the DD simulation. Dissolved iron concentrations above 100 m in the SD simulation declines slightly on the equator and increases somewhat off the equator. Conversely, the DD simulation broadly exhibits elevated dissolved iron concentrations. This suggests that the projected contraction of iron limitation/expansion of macronutrient limitation under DD conditions is attributable to both an increase in iron availability and decrease in macronutrients. Absolute changes in nitrate and dissolved iron are shown in Figure S5 in Supporting Information S1 for reference. PP generally decreases throughout much of the Pacific in both the DD and SD simulations under SSP5-8.5 (Figure 3). However, the DD simulation exhibits a pronounced NPP increase throughout most of the central and eastern equatorial Pacific, and a similarly pronounced decrease in adjacent westward and poleward waters (Figure 3c). That is, DD ultimately reinforces zonal and meridional primary productivity gradients present in the historical climatology (Figure S6 in Supporting Information S1). To illustrate, end-of-21st century productivity in the eastern equatorial Pacific (Niño3: 5°N–5°S, 150°W–90°W; indicated in Figure S6a in Supporting Information S1) increased by 22.0 mg C m⁻² day⁻¹ under DD, a 2.7% increase relative to historical levels. In contrast, productivity in the western equatorial Pacific (5°N–5°S, 160°–180°E; indicated in Figure S6a in Supporting Information S1) declined by –88.0 mg C m⁻² day⁻¹ (17.9% decline). NPP exhibits a more zonally uniform decline in the SD simulation at –30.0 mg C m⁻² day⁻¹ (3.7% decline) and –35.1 mg C m⁻² day⁻¹ (7.2% decline) in the eastern and western equatorial Pacific, respectively.

Spatially, changes in 100 m POC flux (Figures 3d–3f) mirror changes in NPP but are generally more negative across the Pacific. POC flux changed by –3.7 mg C m⁻² day⁻¹ (4.3% decline) and –9.0 mg C m⁻² day⁻¹ (27% decline) in the eastern and western equatorial Pacific, respectively in the DD simulation and by –10.0 mg C m⁻² day⁻¹ (11.8% decline) and –5.2 mg C m⁻² day⁻¹ (16.2% decline) in the eastern and western equatorial Pacific, respectively in the SD simulation. All of the numerical changes reported in this section are statistically significant (student *t*-test, *p* < 0.001). Any effect of these changes in the carbon flux on the eastern equatorial Pacific hypoxic zone, however, were difficult to discern because low frequency (>50 years) variability and model drift in subsurface layers dominate projected changes (Text S4, Figure S8 and S9 in Supporting Information S1).

4. Discussion

Here we show that coupling the air-sea transfer of mineral aerosols by permitting dynamic deposition of soluble iron plays an important role in future projections of tropical Pacific phytoplankton nutrient limitation and primary production. While a formal attribution of dust deposition drivers is beyond the scope of this study, it is clear that interdependent shifts in precipitation and desertification (i.e., decreasing soil moisture; Figure 1, rows 1–2) become more pronounced in higher radiative forcing scenarios. Comparison to the SD simulation (with static iron deposition) shows how the increase in soluble iron deposition in the tropical Pacific predicted by the DD simulation affects upper ocean biogeochemistry (Figure 2a vs. Figure 2b). With DD, the area of tropical Pacific iron limitation recedes and the contrasting increase (decrease) in depth-integrated primary production in the eastern (western) Pacific become more pronounced (Figure 1, rows 6–7).

While projections of increasing equatorial Pacific dust deposition emerge from a complex chain of processes across terrestrial, atmospheric, and ocean components, it must be emphasized that these only partly resolve the diversity of processes that may impact soluble iron delivery and subsequent biogeochemical responses. Several studies, for example, have explored the impacts of projected increases in wildfires, biomass burning, and trends in industrial inputs (e.g., Bergas-Massó et al., 2023; Hamilton et al., 2020b; Matsui et al., 2018), which could further enhance the patterns discussed herein. Also, ESM4.1 does not resolve potential effects of changing atmospheric chemistry on iron solubility (e.g., Baker et al., 2021; Bergas-Massó et al., 2023; Liu et al., 2022), nor does it account for changes in iron content or dust minerality in different source regions (e.g., Bergas-Massó et al., 2022; Journet et al., 2008; Nickovic et al., 2012; Schroth et al., 2009). Finally, while the biogeochemical component enlisted herein is comprehensive relative to most CMIP6 models (Séférian et al., 2020) it still simplifies many aspects of oceanic iron dynamics, including ligand and photochemical dynamics (Tagliabue & Völker, 2011; Tagliabue et al., 2016; Völker & Tagliabue, 2015).

CMIP6 models generally project increasing ocean stratification and decreased nitrate levels in the euphotic zone through the 21st century under SSP5-8.5 (Kwiatkowski et al., 2020). Increased stratification reduces mixing in the euphotic zone, and consequently limits the supply of nutrients, causing reduced levels of phytoplankton

productivity in the tropical oceans (e.g., Behrenfeld et al., 2006; Doney, 2006). This process also impacts the iron supply from below the surface layer, but not supply from prominent depositional sources. As such, we might expect phytoplankton growth to become more macro-nutrient limited as phosphate and nitrate become less available in the upper ocean. As there is no long-term increase in the atmospheric source of iron in the SD simulation, the slight contraction of future iron limitation in the central Pacific is likely attributable to this mechanism. Conversely, the larger eastward recession of iron limitation in the future DD simulation is attributable to the combination of increased iron availability and macronutrient scarcity, consistent with past perturbation experiments. As demonstrated in Hamilton et al. (2020a), enhanced productivity in the equatorial Pacific consumes dissolved macronutrients thus reducing their concentrations in surface waters that are subsequently subducted into the subtropical nutricline (Figures 2f and 2h). This leads to a more pronounced macronutrient limitation-driven decline in productivity in the DD versus SD simulation in downstream (western) and subducted (off-equatorial) regions. The differences in the change in NPP (Figure 3c), positive in the equatorial and negative in the western and off-equatorial Pacific regions, is consistent with the discrepancy between dynamic and static dust simulations in the extent of phytoplankton iron limitation (Figures 2c and 2d). Specifically, elevated iron deposition stimulates productivity in regions where iron scarcity continues to be the primary limitation of phytoplankton growth but not in regions that transitioned to being macronutrient-limited (e.g., J. K. Moore et al., 2004). The geographic pattern of this signal is echoed in changes in phytoplankton community size structure (Figures S7c and S7h in Supporting Information S1) and POC flux (Figure 3f), which illustrates the cascading trophic effects of dynamic dust deposition and resultant shift in nutrient limitations. Specifically, the more pronounced increase in small phytoplankton in the western Pacific is consistent with the effects of macro-nutrient limitation impacts on phytoplankton cell-size (Peter & Sommer, 2013). Several studies have demonstrated similar compensatory patterns in tropical Pacific biogeochemical sensitivity to perturbations in dust deposition and iron cycling. J. K. Moore et al. (2004), for example, describe a reduction in the extent of iron limitation in the central equatorial Pacific under elevated rates of dust deposition (i.e., scaled-up globally by factors of 2, 4, and 10). At the global scale, the values they report show increasing primary production and sinking particulate organic matter with increasing dust deposition. Conversely, we see declines (future—historical) in global primary production and particulate organic carbon export, regardless of the iron deposition simulation (Table S1 in Supporting Information S1). This may be attributable to the fact that, unlike the idealized treatments in J. K. Moore et al. (2004), the change in iron deposition in our simulations varies spatially, exhibiting a 2- to 3-fold increase only in the tropical Pacific ocean (Figure 1). As such, the globally integrated changes in dust and iron deposition are comparatively smaller (<1.1x; Table S1 in Supporting Information S1) than those in J. K. Moore et al. (2004) with other drivers being more important in governing projected changes in total global primary production and carbon export.

Hamilton et al. (2020a) similarly reported reduced phytoplankton iron limitation in the central tropical Pacific under elevated future soluble iron delivery accompanied by an increase (decrease) in NPP and POC flux in the eastern (western) tropical Pacific. However, where Hamilton et al. (2020a) specifically tested sensitivity to different prescribed levels of surface sources of soluble iron under constant meteorology, our results reflect dynamically consistent changes in the whole earth system, which permits analysis of co-evolving and interacting signals. While projected increases in Pacific iron deposition herein (~150%–200%, Figure 1, row 5) are comparable to Hamilton et al. (2020a, Figure 2a), ESM4.1 enables exploration of the integrated effects of interlinked changes in dust emissions, transport, precipitation and stratification on ocean nutrient limitation and productivity. However, unlike Hamilton et al. (2020a), our study does not consider the direct effects of fires as sources for dust emissions or changes in industrial emissions. Given the substantial contribution of fires to projected dust deposition in the equatorial Pacific in Hamilton et al. (2020a), the change in soluble iron deposition projected in ESM4.1 (Figure 1, row 5) for the equatorial Pacific region could be an underestimate.

Tagliabue et al. (2020) tested NPP and upper trophic level sensitivity to parameterizations of phytoplankton iron uptake (as opposed to the impact of variable iron deposition) and observed similar changes in the spatial extent of iron versus macronutrient limitation over time. The anomaly in NPP of their study is geographically similar (i.e., positive in the eastern equatorial/negative in the western and off-equatorial Pacific) to that observed in Figure 3c of this study, illustrating how different tunings of iron cycling project similar impacts on the position of the tropical Pacific iron limitation front and subsequent, down-stream biogeochemical responses. Tagliabue et al. (2020) note that NPP was more resilient to climate change (i.e., declined less or even increased in the equatorial Pacific) when phytoplankton remained iron limited (as opposed to transitioning to macronutrient limited). Similarly, the portion of the equatorial Pacific that remained at least weakly iron-limited in our future projections experienced

the largest NPP increases under climate change (Figure 1, rows 6–7; Table S1 in Supporting Information S1). Even without increasing iron deposition (i.e., under SD), NPP in this iron-limited region was resilient to climate change (Figure 3; Table S2 in Supporting Information S1). This is broadly consistent with the aforementioned mechanism described in J. K. Moore et al. (2004) in that persistence of phytoplankton iron-limitation would sustain the positive impact of iron deposition on primary production. It also further suggests that areas of strong iron limitation may be particularly resilient to stratification-driven climate change impacts on NPP (Tagliabue et al., 2020).

Implementation of dynamic iron deposition had only a minor effect on model skill in representing ocean biogeochemistry; historical simulations exhibit very similar dust/iron deposition, regardless of whether they are climatologically- prescribed or dynamically coupled to atmospheric conditions (i.e., the biggest projected differences herein have yet to be observed). In terms of variability, however, Lim et al. (2022) found that the amplitude of negative chlorophyll anomalies in onset and during mature El Niño events is weaker with DD than SD, but the amplitude of positive chlorophyll responses in the decaying El Niño is stronger in DD than SD, with DD ameliorating the negative influence of El Niño on both iron and chlorophyll relative to SD. Unfortunately, the satellite chlorophyll record is currently not long enough to say whether the DD interactions are an improvement. Séférian et al. (2020) did find that the four ESMs that incorporated dynamic dust deposition demonstrated improved model performance in terms of CMIP5 versus CMIP6 model correlation with observations of surface chlorophyll and oxygen concentration at 150 m depth. However, these improvements were subtle in some cases and are ultimately impossible to attribute to iron deposition alone as each successive generation of ESM incorporates numerous new model developments.

Discrepancies in ESM representation of iron deposition to the ocean could contribute to inter-model disagreement in regional projections of ocean biogeochemistry. Across CMIP5 and CMIP6 models, Tagliabue et al. (2021) demonstrate that some of the largest standard deviations and ranges in projections of primary production occur in the equatorial Pacific, which is the region where we see the greatest influence of implementing dynamic versus static dust deposition on phytoplankton iron limitation (Figure 2a vs. Figure 2b). Indeed, the multi-model mean change in equatorial Pacific NPP in Tagliabue et al. (2021) looks more like the change in primary production exhibited in our SD simulation than the DD simulation (Figure 3a vs. Figure 3b, replotted in Figure S10 in Supporting Information S1 to facilitate comparison with Tagliabue et al. (2021)). Tagliabue et al. (2021) highlight model parameterization of phytoplankton nutrient limitation as an important source of uncertainty in regional projections of primary production across ESMs; We would add that the representation of variable dust deposition is also important, particularly under higher radiative forcing scenarios (Figure 1).

5. Conclusions

While the method of ocean iron deposition (dynamically coupled vs. climatologically prescribed) has little effect on preindustrial and historical simulations of ocean BGC conditions, ESM-evolution toward more comprehensive representation of land-air-sea interactions (e.g., dynamic iron deposition) has critical implications for marine ecosystems in a changing climate. Specifically, under increasing radiative forcing conditions, representation of ocean iron deposition mechanisms affects basin-scale distribution of modeled primary production, which has nutritional implications for higher trophic level organisms, including lucrative fisheries.

Presently, static (as opposed to dynamically coupled) iron deposition is more common in CMIP6 ESMs. This may be adequate for projecting future conditions at locations where dust deposition remains relatively unchanged. However, these model configuration choices could have important implications for tropical Pacific Ocean productivity under higher emission scenarios, wherein land use, elevated temperature and changes in precipitation distribution substantially alter the transfer of mineral aerosols, and thus nutrient delivery, to the surface ocean.

Data Availability Statement

Model output generated for CMIP6 is available on the Earth System Grid Federation (<https://esgdata.gfdl.noaa.gov/search/cmip6-gfdl/>). CMIP6 model data produced by NOAA-GFDL is licensed under a Creative Commons Attribution 4.0 International License (CC BY 4.0, <https://creativecommons.org/licenses/>). Consult <https://pcmdi.llnl.gov/CMIP6/TermsOfUse> for terms of use governing CMIP6 output, including citation requirements and proper acknowledgment. Further information about this data, including some limitations, can be found via the

further_info_url (recorded as a global attribute in this file). The data producers and data providers make no warranty, either express or implied, including, but not limited to, warranties of merchantability and fitness for a particular purpose. All liabilities arising from the supply of the information (including any liability arising in negligence) are excluded to the fullest extent permitted by law. Model output that is not available through CMIP6 (i.e., output from the static dust simulation and dynamic variables not served through CMIP) has been archived at <https://doi.org/10.5281/zenodo.8341680>. Model diagnostics are saved to netCDF files and further post-processing was conducted using NCO (<https://nco.sourceforge.net/>; Zender et al., 2008). Analyses were coded in Python using Jupyter notebooks that are also included in the Zenodo archive, along with a list of the packages comprising the Python environment. To highlight a few, figures were rendered using Matplotlib (<https://matplotlib.org/>; Hunter, 2007), maps were configured using Cartopy (<https://scitools.org.uk/cartopy/docs/latest/>; Elson et al., 2023), and statistical analyses were conducted using SciPy (<https://scipy.org/>; Virtanen et al., 2020).

Acknowledgments

The authors thank Elise Olson and Songmiao Fan for their comments and suggestions via an internal review of the manuscript. We also appreciate the comments provided by two anonymous reviewers who helped improve the quality of the paper. H.-G. Lim was supported under award NA18OAR4320123 from the National Oceanic and Atmospheric Association, U.S. Department of Commerce.

References

- Baker, A. R., & Croot, P. L. (2010). Atmospheric and marine controls on aerosol iron solubility in seawater. *Marine Chemistry*, 120(1–4), 4–13. <https://doi.org/10.1016/j.marchem.2008.09.003>
- Baker, A. R., Kanakidou, M., Nenes, A., Myriokefalitakis, S., Croot, P. L., Duce, R. A., et al. (2021). Changing atmospheric acidity as a modulator of nutrient deposition and ocean biogeochemistry. *Science Advances*, 7(28), eabd8800. <https://doi.org/10.1126/sciadv.abd8800>
- Behrenfeld, M. J., O'Malley, R. T., Siegel, D. A., McClain, C. R., Sarmiento, J. L., Feldman, G. C., et al. (2006). Climate-driven trends in contemporary ocean productivity. *Nature*, 444(7120), 752–755. <https://doi.org/10.1038/nature05317>
- Bergas-Massó, E., Gonçalves Ageitos, M., Myriokefalitakis, S., Miller, R. L., & García-Pando, C. P. (2022). How does the use of different soil mineralogical Atlases impact soluble iron deposition estimates? In C. Mensink & O. Jorba (Eds.), *Air pollution modeling and its application XXVIII. ITM 2021. Springer proceedings in complexity*. Springer. https://doi.org/10.1007/978-3-031-12786-1_34
- Bergas-Massó, E., Gonçalves Ageitos, M., Myriokefalitakis, S., Miller, R. L., van Noije, T., Le Sager, P., et al. (2023). Pre-industrial, present and future atmospheric soluble iron deposition and the role of aerosol acidity and oxalate under CMIP6 emissions. *Earth's Future*, 11(6), e2022EF003353. <https://doi.org/10.1029/2022EF003353>
- Boyd, P., Watson, A., Law, C. S., Abraham, E. R., Trull, T., Murdoch, R., et al. (2000). A mesoscale phytoplankton bloom in the polar Southern Ocean stimulated by iron fertilization. *Nature*, 407(6805), 695–702. <https://doi.org/10.1038/35037500>
- Burrell, A. L., Evans, J. P., & De Kauwe, M. G. (2020). Anthropogenic climate change has driven over 5 million km² of drylands towards desertification. *Nature Communications*, 11(1), 3853. <https://doi.org/10.1038/s41467-020-17710-7>
- Coale, K. H., Johnson, K. S., Fitzwater, S. E., Gordon, R. M., Tanner, S., Chavez, F. P., et al. (1996). A massive phytoplankton bloom induced by an ecosystem-scale iron fertilization experiment in the equatorial Pacific Ocean. *Nature*, 383(6600), 495–501. <https://doi.org/10.1038/383495a0>
- Danabasoglu, G., Lamarque, J.-F., Bacmeister, J., Bailey, D. A., DuVivier, A. K., Edwards, J., et al. (2020). The community Earth System Model version 2 (CESM2). *Journal of Advances in Modeling Earth Systems*, 12, e2019MS001916. <https://doi.org/10.1029/2019MS001916>
- Doney, S. (2006). Plankton in a warmer world. *Nature*, 444(7120), 695–696. <https://doi.org/10.1038/444695a>
- Duce, R. A., & Tindale, N. W. (1991). Atmospheric transport of iron and its deposition in the ocean. *Limnology & Oceanography*, 36(8), 1715–1726. <https://doi.org/10.4319/lo.1991.36.8.1715>
- Dunne, J. P., Horowitz, L. W., Adcroft, A. J., Ginoux, P., Held, I. M., John, J. G., et al. (2020). The GFDL Earth System Model Version 4.1 (GFDL-ESM 4.1): Overall coupled model description and simulation characteristics. *Journal of Advances in Modeling Earth Systems*, 12(11), e2019MS002015. <https://doi.org/10.1029/2019ms002015>
- Elrod, V. A., Berelson, W. M., Coale, K. H., & Johnson, K. S. (2004). The flux of iron from continental shelf sediments: A missing source for global budgets. *Geophysical Research Letters*, 31(12), L12307. <https://doi.org/10.1029/2004GL020216>
- Elson, P., De Andrade, E. S., Lucas, G., May, R., Hattersley, R., Campbell, E., et al. (2023). SciTools/cartopy: v0.22.0 (Version v0.22.0) [Computer software]. Zenodo. <https://doi.org/10.5281/ZENODO.8216315>
- Evans, S., Ginoux, P., Malyshev, S., & Shevliakova, E. (2016). Climate-vegetation interaction and amplification of Australian dust variability. *Geophysical Research Letters*, 43(22), 11823–11830. <https://doi.org/10.1002/2016GL071016>
- Eyring, V., Bony, S., Meehl, G. A., Senior, C. A., Stevens, B., Stouffer, R. J., & Taylor, K. E. (2016). Overview of the Coupled Model Inter-comparison Project Phase 6 (CMIP6) experimental design and organization. *Geoscientific Model Development*, 9(5), 1937–1958. <https://doi.org/10.5194/gmd-9-1937-2016>
- Gillette, D. A., & Passi, R. (1988). Modeling dust emission caused by wind erosion. *Journal of Geophysical Research*, 93(D11), 14233–14242. <https://doi.org/10.1029/JD093iD11p14233>
- Hajima, T., Watanabe, M., Yamamoto, A., Tatebe, H., Noguchi, M. A., Abe, M., et al. (2020). Development of the MIROC-ES2L Earth system model and the evaluation of biogeochemical processes and feedbacks. *Geoscientific Model Development*, 13(5), 2197–2244. <https://doi.org/10.5194/gmd-13-2197-2020>
- Hamilton, D. S., Moore, J. K., Arneeth, A., Bond, T. C., Carslaw, K. S., Hantson, S., et al. (2020a). Impact of changes to the atmospheric soluble iron deposition flux on ocean biogeochemical cycles in the Anthropocene. *Global Biogeochemical Cycles*, 34(3), e2019GB006448. <https://doi.org/10.1029/2019GB006448>
- Hamilton, D. S., Scanza, R. A., Rathod, S. D., Bond, T. C., Kok, J. F., Li, L., et al. (2020b). Recent (1980 to 2015) trends and variability in daily-to-interannual soluble iron deposition from dust, fire, and anthropogenic sources. *Geophysical Research Letters*, 47(17), e2020GL089688. <https://doi.org/10.1029/2020GL089688>
- Huang, J., Zhang, G., Zhang, Y., Guan, X., Wei, Y., & Guo, R. (2020). Global desertification vulnerability to climate change and human activities. *Land Degradation & Development*, 31(11), 1380–1391. <https://doi.org/10.1002/ldr.3556>
- Hunter, J. D. (2007). Matplotlib: A 2D graphics environment. *Computing in Science & Engineering*, 9(3), 90–95.
- John, J. G., Blanton, C., McHugh, C., Radhakrishnan, A., Rand, K., Vahlenkamp, H., et al. (2018). NOAA-GFDL GFDL-ESM4 model output prepared for CMIP6 ScenarioMIP ssp585. Version 20180701. Earth System Grid Federation. <https://doi.org/10.22033/ESGF/CMIP6.8706>
- Johnson, K. S. (2001). Iron supply and demand in the upper ocean: Is extraterrestrial dust a significant source of bioavailable iron? *Global Biogeochemical Cycles*, 15(1), 61–63. <https://doi.org/10.1029/2000GB001295>

- Journet, E., Desboeufs, K. V., Caqueneau, S., & Colin, J.-L. (2008). Mineralogy as a critical factor of dust iron solubility. *Geophysical Research Letters*, 35(7), L07805. <https://doi.org/10.1029/2007GL031589>
- Krachler, R., Jirsa, F., & Ayromlou, S. (2005). Factors influencing the dissolved iron input by river water to the open ocean. *Biogeosciences*, 2(4), 311–315. <https://doi.org/10.5194/bg-2-311-2005>
- Krasting, J. P., John, J. G., Blanton, C., McHugh, C., Nikonov, S., Radhakrishnan, A., et al. (2018a). NOAA-GFDL GFDL-ESM4 model output prepared for CMIP6 CMIP historical. Version 20190726. Earth System Grid Federation. <https://doi.org/10.22033/ESGF/CMIP6.8597>
- Krasting, J. P., John, J. G., Blanton, C., McHugh, C., Nikonov, S., Radhakrishnan, A., et al. (2018b). NOAA-GFDL GFDL-ESM4 model output prepared for CMIP6 CMIP piControl. Version 20180701. Earth System Grid Federation. <https://doi.org/10.22033/ESGF/CMIP6.8669>
- Kwiatkowski, L., Torres, O., Bopp, L., Aumont, O., Chamberlain, M., Christian, J. R., et al. (2020). Twenty-first century ocean warming, acidification, deoxygenation, and upper-ocean nutrient and primary production decline from CMIP6 model projections. *Biogeosciences*, 17(13), 3439–3470. <https://doi.org/10.5194/bg-17-3439-2020>
- Lee, J.-Y., Marotzke, J., Bala, G., Cao, L., Corti, S., Dunne, J. P., et al. (2021). Future global climate: Scenario-based projections and NearTerm information. In V. Masson-Delmotte, P. Zhai, A. Pirani, S. L. Connors, C. Péan, S. Berger, et al. (Eds.), *Climate change 2021: The physical science basis. Contribution of working group I to the Sixth assessment report of the intergovernmental panel on climate change* (pp. 553–672). Cambridge University Press. <https://doi.org/10.1017/9781009157896.006>
- Liebig, J. (1840). *Chemistry and its applications to agriculture and physiology* (p. 414). Taylor and Walton.
- Lim, H.-G., Dunne, J. P., Stock, C. A., Ginoux, P., John, J. G., & Krasting, J. (2022). Oceanic and atmospheric drivers of post-El-Niño chlorophyll rebound in the equatorial Pacific. *Geophysical Research Letters*, 49(5), e2021GL096113. <https://doi.org/10.1029/2021GL096113>
- Liu, L., Li, W., Lin, Q., Wang, Y., Zhang, J., Zhu, Y., et al. (2022). Size-dependent aerosol iron solubility in an urban atmosphere. *npj Climate and Atmospheric Science*, 5(1), 53. <https://doi.org/10.1038/s41612-022-00277-z>
- Mahowald, N. M., Baker, A. R., Bergametti, G., Brooks, N., Duce, R. A., Jickells, T. D., et al. (2005). Atmospheric global dust cycle and iron inputs to the ocean. *Global Biogeochemical Cycles*, 19(4), GB4025. <https://doi.org/10.1029/2004GB002402>
- Mahowald, N. M., Engelstaedter, S., Luo, C., Sealy, A., Artaxo, P., Benitez-Nelson, C., et al. (2009). Annual review of atmospheric iron deposition: Global distribution, variability, and human perturbations. *Annual Review of Marine Science*, 1, 245–278. <https://doi.org/10.1146/annurev.marine.010908.163727>
- Martin, J. H. (1990). Glacial-interglacial CO₂ change: The iron hypothesis. *Paleoceanography*, 5(1), 1–13. <https://doi.org/10.1029/PA005i001p00001>
- Matsui, H., Mahowald, N. M., Moteki, N., Hamilton, D. S., Ohata, S., Yoshida, A., et al. (2018). Anthropogenic combustion iron as a complex climate forcer. *Nature Communications*, 9(1), 1593. <https://doi.org/10.1038/s41467-018-03997-0>
- Meskhidze, N., Chameides, W. L., & Nenes, A. (2005). Dust and pollution: A recipe for enhanced ocean fertilization? *Journal of Geophysical Research*, 110(D3), D03301. <https://doi.org/10.1029/2004JD005082>
- Moore, C. M., Mills, M. M., Arrigo, K. R., Berman-Frank, I., Bopp, L., Boyd, P. W., et al. (2013). Processes and patterns of oceanic nutrient limitation. *Nature Geoscience*, 6(9), 701–710. <https://doi.org/10.1038/ngeo1765>
- Moore, J. K., Doney, S. C., & Lindsay, K. (2004). Upper ocean ecosystem dynamics and iron cycling in a global three-dimensional model. *Global Biogeochemical Cycles*, 18(4), GB4028. <https://doi.org/10.1029/2004GB002220>
- Nickovic, S., Vukovic, A., Vujadinovic, M., Djurdjevic, V., & Pejanovic, G. (2012). Technical Note: High-resolution mineralogical database of dust-productive soils for atmospheric dust modeling. *Atmospheric Chemistry and Physics*, 12(2), 845–855. <https://doi.org/10.5194/acp-12-845-2012>
- O'Neill, B. C., Krieglner, E., Riahi, K., Ebi, K. L., Hallegatte, S., Carter, T. R., et al. (2014). A new scenario framework for climate change research: The concept of shared socioeconomic pathways. *Climatic Change*, 122(3), 387–400. <https://doi.org/10.1007/s10584-013-0905-2>
- O'Neill, B. C., Tebaldi, C., van Vuuren, D. P., Eyring, V., Friedlingstein, P., Hurtt, G., et al. (2016). The Scenario Model Intercomparison Project (ScenarioMIP) for CMIP6. *Geoscientific Model Development*, 9, 3461–3482. <https://doi.org/10.5194/gmd-9-3461-2016>
- Orr, J. C., Najjar, R. G., Aumont, O., Bopp, L., Bullister, J. L., Danabasoglu, G., et al. (2017). Biogeochemical protocols and diagnostics for the CMIP6 ocean model intercomparison project (OMIP). *Geoscientific Model Development*, 10(6), 2169–2199. <https://doi.org/10.5194/gmd-10-2169-2017>
- Peter, K. H., & Sommer, U. (2013). Phytoplankton cell size reduction in response to warming mediated by nutrient limitation. *PLoS One*, 8(9), e71528. <https://doi.org/10.1371/journal.pone.0071528>
- Riahi, K., van Vuuren, D. P., Krieglner, E., Edmonds, J., O'Neill, B. C., Fujimori, S., et al. (2017). The Shared Socioeconomic Pathways and their energy, land use, and greenhouse gas emissions implications: An overview. *Global Environmental Change*, 42, 153–168. <https://doi.org/10.1016/j.gloenvcha.2016.05.009>
- Schroth, A., Crusius, J., Sholkovitz, E., & Bostick, B. C. (2009). Iron solubility driven by speciation in dust sources to the ocean. *Nature Geoscience*, 2(5), 337–340. <https://doi.org/10.1038/ngeo501>
- Schulz, M., Prospero, J. M., Baker, A. R., Dentener, F., Ickes, L., Liss, P. S., et al. (2012). Atmospheric transport and deposition of mineral dust to the ocean: Implications for research needs. *Environmental Science & Technology*, 46(19), 10390–10404. <https://doi.org/10.1021/es300073u>
- Séférian, R., Berthet, S., Yool, A., Palmiéri, J., Bopp, L., Tagliabue, A., et al. (2020). Tracking improvement in simulated marine biogeochemistry between CMIP5 and CMIP6. *Current Climate Change Reports*, 6(3), 95–119. <https://doi.org/10.1007/s40641-020-00160-0>
- Sellar, A. A., Jones, C. G., Mulcahy, J. P., Tang, Y., Yool, A., Wiltshire, A., et al. (2019). UKESM1: Description and evaluation of the U.K. Earth system model. *Journal of Advances in Modeling Earth Systems*, 11(12), 4513–4558. <https://doi.org/10.1029/2019MS001739>
- Stock, C. A., Dunne, J. P., Fan, S., Ginoux, P., John, J. G., Krasting, J. P., et al. (2020). Ocean biogeochemistry in GFDL's earth system model 4.1 and its response to increasing atmospheric CO₂. *Journal of Advances in Modeling Earth Systems*, 12(10), e2019MS002043. <https://doi.org/10.1029/2019MS002043>
- Tagliabue, A., Aumont, O., DeAth, R., Dunne, J. P., Dutkiewicz, S., Galbraith, E., et al. (2016). How well do global ocean biogeochemistry models simulate dissolved iron distributions? *Global Biogeochemical Cycles*, 30(2), 149–174. <https://doi.org/10.1002/2015GB005289>
- Tagliabue, A., Barrier, N., Du Pontavice, H., Kwiatkowski, L., Aumont, O., Bopp, L., et al. (2020). An iron cycle cascade governs the response of equatorial Pacific ecosystems to climate change. *Global Change Biology*, 26(11), 6168–6179. <https://doi.org/10.1111/gcb.15316>
- Tagliabue, A., Bopp, L., Dutay, J.-C., Bowie, A. R., Chever, F., Jean-Baptiste, P., et al. (2010). Hydrothermal contribution to the oceanic dissolved iron inventory. *Nature Geoscience*, 3(4), 252–256. <https://doi.org/10.1038/ngeo818>
- Tagliabue, A., Bowie, A. R., Boyd, P. W., Buck, K. N., Johnson, K. S., & Saito, M. A. (2017). The integral role of iron in ocean biogeochemistry. *Nature*, 543(7643), 51–59. <https://doi.org/10.1038/nature21058>
- Tagliabue, A., Kwiatkowski, L., Bopp, L., Butenschön, M., Cheung, W., Lengaigne, M., & Vialard, J. (2021). Persistent uncertainties in ocean net primary production climate change projections at regional scales raise challenges for assessing impacts on ecosystem services. *Frontiers in Climate*, 3, 738224. <https://doi.org/10.3389/fclim.2021.738224>

- Tagliabue, A., & Völker, C. (2011). Towards accounting for dissolved iron speciation in global ocean models. *Biogeosciences*, 8(10), 3025–3039. <https://doi.org/10.5194/bg-8-3025-2011>
- Tagliabue, A., Williams, R. G., Rogan, N., Achterberg, E. P., & Boyd, P. W. (2014). A ventilation-based framework to explain the regeneration-scavenging balance of iron in the ocean. *Geophysical Research Letters*, 41(20), 7227–7236. <https://doi.org/10.1002/2014GL061066>
- Virtanen, P., Gommers, R., Oliphant, T. E., Haberland, M., Reddy, T., Cournapeau, D., et al. (2020). SciPy 1.0: Fundamental algorithms for scientific computing in Python. *Nature Methods*, 17(3), 261–272. <https://doi.org/10.1038/s41592-019-0686-2>
- Völker, C., & Tagliabue, A. (2015). Modeling organic iron-binding ligands in a three-dimensional biogeochemical ocean model. *Marine Chemistry*, 173, 67–77. <https://doi.org/10.1016/j.marchem.2014.11.008>
- Zender, C. S. (2008). Analysis of self-describing gridded geoscience data with netCDF Operators (NCO). *Environmental Modelling & Software*, 23(10–11), 1338–1342. <https://doi.org/10.1016/j.envsoft.2008.03.004>

References From the Supporting Information

- Busecke, J. J. M., Resplandy, L., Ditkovsky, S. J., & John, J. G. (2022). Diverging fates of the Pacific Ocean oxygen minimum zone and its core in a warming world. *AGU Advances*, 3(6), e2021AV000470. <https://doi.org/10.1029/2021AV000470>
- Deutsch, C., Ferrel, A., Seibel, B., Pörtner, H. O., & Huey, R. B. (2015). Climate change tightens a metabolic constraint on marine habitats. *Science*, 348(6239), 1132–1135. <https://doi.org/10.1126/science.aaa1605>